BASIC SCIENCE

Suppression of Sleep Spindle Rhythmogenesis in Mice with Deletion of $Ca_V3.2$ and $Ca_V3.3$ T-type Ca^{2+} Channels

Chiara Pellegrini, MSc; Sandro Lecci, MSc; Anita Lüthi, PhD; Simone Astori, PhD

Department of Fundamental Neurosciences, University of Lausanne, Lausanne, Switzerland

Study Objectives: Low-threshold voltage-gated T-type Ca^{2+} channels (T-channels or Ca_V3 channels) sustain oscillatory discharges of thalamocortical (TC) and *nucleus Reticularis thalami* (nRt) cells. The $Ca_V3.3$ subtype dominates nRt rhythmic bursting and mediates a substantial fraction of spindle power in the NREM sleep EEG. $Ca_V3.2$ channels are also found in nRt, but whether these contribute to nRt-dependent spindle generation is unexplored. We investigated thalamic rhythmogenesis in mice lacking this subtype in isolation ($Ca_V3.2$KO mice) or in concomitance with $Ca_V3.3$ deletion (Ca_V3.double-knockout (DKO) mice).
Methods: We examined discharge characteristics of thalamic cells and intrathalamic evoked synaptic transmission in brain slices from wild-type, $Ca_V3.2$KO and Ca_V3.DKO mice through patch-clamp recordings. The sleep profile of freely behaving $Ca_V3.2$KO and Ca_V3.DKO mice was assessed by polysomnographic recordings.
Results: $Ca_V3.2$ channel deficiency left nRt discharge properties largely unaltered, but additional deletion of $Ca_V3.3$ channels fully abolished low-threshold whole-cell Ca^{2+} currents and bursting, and suppressed burst-mediated inhibitory responses in TC cells. Ca_V3.DKO mice had more fragmented sleep, with shorter NREM sleep episodes and more frequent microarousals. The NREM sleep EEG power spectrum displayed a relative suppression of the σ frequency band (10–15 Hz), which was accompanied by an increase in the δ band (1–4 Hz).
Conclusions: Consistent with previous findings, $Ca_V3.3$ channels dominate nRt rhythmogenesis, but the lack of $Ca_V3.2$ channels further aggravates neuronal, synaptic, and EEG deficits. Therefore, $Ca_V3.2$ channels can boost intrathalamic synaptic transmission, and might play a modulatory role adjusting the relative presence of NREM sleep EEG rhythms.
Keywords: sleep spindles, sleep architecture, nucleus Reticularis thalami
Citation: Pellegrini C, Lecci S, Lüthi A, Astori S. Suppression of sleep spindle rhythmogenesis in mice with deletion of $Ca_V3.2$ and $Ca_V3.3$ T-type Ca^{2+} channels. *SLEEP* 2016;39(4):875–885.

Significance
Sleep spindles are recurrent brain electrical oscillations typical for non-rapid-eye-movement sleep that protect the sleeping brain from external disturbance, sustain memory reinforcement in neuronal circuits and appear to be altered in several psychiatric disorders. We succeeded in suppressing sleep spindles in mice by genetically deleting the two low-voltage-gated Ca^{2+} channels responsible for rhythmic electrical discharges of cells in the *nucleus Reticularis thalami*, also known as the thalamic spindle pacemaker. Our findings help dissecting the genetic make-up of sleep rhythmogenesis and offer a mouse model to examine the pathophysiological consequences of disrupting sleep spindles.

INTRODUCTION

Low voltage-gated T-type Ca^{2+} channels (T-channels) enable neurons to produce low-threshold discharges that are essential for the generation of sleep rhythms, but that occur also in motor control and olfaction.[1–6] Furthermore, T-channels may lead to aberrant bursting in neurons exposed to abnormal electrical activity.[1,7,8] T-channels are encoded by three genes, *CACNA1g*, *CACNA1h* and *CACNA1i* that give rise to the subtypes $Ca_V3.1$, $Ca_V3.2$, and $Ca_V3.3$, respectively, characterized by different biophysical properties and expression patterns.[9,10] T-channels are most abundant in thalamus, where they exhibit regional specificity: whereas $Ca_V3.1$ channel mRNA is restricted to excitatory thalamocortical (TC) cells, e.g., in the ventrobasal nucleus (VB), mRNA for both $Ca_V3.2$ and $Ca_V3.3$ channels is present in the *nucleus Reticularis thalami* (nRt),[10,11] a shell of GABAergic cells modulating the information flow in the thalamocortical system.[12]

Genetic manipulations of Ca_V3 channels have yielded substantial insight into the mechanisms of oscillatory activity of neuronal cells. However, in contrast to the well-established role of T-channels in single-cell burst discharge, how these channels contribute to network rhythmic activity has only partially progressed since the generation of knock-out (KO) animals. Furthermore, in at least some cases, the relation between the cellular effects of T-channel subtype deletion and the purported role of burst discharges in EEG rhythms remains obscure. For example, $Ca_V3.1$ channels are clearly responsible for low-threshold bursting in TC cells. However, both increases and decreases in the δ power (1–4 Hz) of the NREM sleep EEG were observed in animals lacking $Ca_V3.1$ channels.[13,14] Therefore, a long-standing tenet on the TC cell clock-like burst discharges as basis for the EEG δ rhythm[15,16] could not yet be confirmed based on Ca_V3 channel genetics.

We have previously shown that the $Ca_V3.3$ subtype is the major source of low-threshold Ca^{2+} spikes in nRt cell dendrites.[17] In $Ca_V3.3$KO mice, nRt repetitive burst discharges were strongly reduced, leading to an impaired inhibitory drive onto TC cells. Furthermore, consistent with the previously recognized implication of the nRt in sleep spindle pacemaking, EEG power in the σ frequency range (10–15 Hz) was weakened at transitions between NREM and REM sleep in $Ca_V3.3$KO animals. There were no other major changes in EEG frequency bands, which indicated a $Ca_V3.3$-specific decrease in sleep spindle rhythmogenesis.[17]

Although $Ca_V3.3$-deficiency led to a reduction in sleep spindles, a substantial portion of power increase remained present in the σ frequency band at NREM sleep exit, suggesting that other cellular mechanisms contributing to these thalamocortical rhythms exist. A major candidate is the $Ca_V3.2$-current that has been identified in nRt cells,[18] and that appears to be the target of several modulatory extracellular and intracellular signaling molecules.[19] To date, $Ca_V3.2$ channels are implicated in peripheral nociception and neuropathic pain, and might be involved in

specific forms of thalamic processing, e.g., relay of nociceptive inputs.[20–22] In addition, the expression of $Ca_V3.2$ channels can be modified in pathological conditions, e.g., in animal models of epilepsy.[7] Whether and how $Ca_V3.2$ channels contribute to thalamic sleep rhythmogenesis has yet not been ascertained.

Here, we examined the consequences of silencing Ca_V3-mediated nRt rhythmogenesis on the EEG profile of mice harboring a deletion of *$Ca_V3.2$* and *$Ca_V3.3$* genes (Ca_V3.DKO). Whereas a lack of the $Ca_V3.2$ subtype alone in $Ca_V3.2$KO mice did not cause major alterations to nRt cellular properties, Ca_V3.DKO mice showed a fully abolished nRt low-threshold spiking and strongly impaired intrathalamic GABAergic transmission. In freely behaving $Ca_V3.2$KO mice, the EEG power spectrum during NREM sleep was indistinguishable from that of wild-type animals. By contrast, in Ca_V3.DKO mice, relative EEG power in the σ frequency range during NREM sleep was suppressed and accompanied by an increase in the δ frequency range. Although Ca_V3.DKO mice spent globally more time in NREM sleep during the light phase, NREM sleep episodes were of shorter duration compared to wild-type animals. Thus, silencing low-threshold bursts in nRt neurons not only affects spindle generation, but also alters slow wave rhythmogenesis, likely due to deficient inhibitory drive onto TC cells.

METHODS

Animal Handling and Genotyping

All procedures were approved by the Veterinary Office of the Canton de Vaud. C57Bl/6J (wild-type), homozygous $Ca_V3.2$KO and homozygous Ca_V3.DKO mice were maintained under a 12:12h light/dark schedule (Zeitgeber time ZT 0: 7AM for animals used for electrophysiological recordings; 9AM for polysomnographic recordings). Homozygous $Ca_V3.2$KO mice were obtained from heterozygous breeders ($Ca_V3.2$*het*) from the *Cacna1h*-KO mouse line,[23] originally generated on a mixed C57Bl/6J-129S3 background that was backcrossed into the C57Bl/6J background for 4 generations and has since been backcrossed into the C57Bl/6J background for over 10 years. Homozygous Ca_V3.DKO mice were obtained by crossing the $Ca_V3.2$KO and the C57Bl/6J-*Cacna1i*-KO ($Ca_V3.3$KO) mouse line.[17] First, $Ca_V3.2$*het*/$Ca_V3.3$*het* mice were generated from $Ca_V3.2$*het* and homozygous $Ca_V3.3$KO mice. Second, $Ca_V3.2$*het*/$Ca_V3.3$*het* were interbred, and the obtained $Ca_V3.2$*het*/$Ca_V3.3$KO mice were selected as final breeders for the generation of Ca_V3.DKO mice. The percentage of homozygous Ca_V3.DKO mice at the time of genotyping (P8-12) was below Mendelian expectation (< 10%), suggesting high perinatal mortality. The genotype was determined by PCR using the following primers (5'–3') for the *CACNA1h* gene, following a protocol provided by Heinz Beck's laboratory at the University of Bonn: CACNA1hF: ATTCAAGGGCTTCCACAGGGTA; CACNA1hR: CATCTCAGGGCCTCTGGACCAC; CACNA1hNeo: GCTAAAGCGCATGCTCCAGACTG, yielding products of 480 bp for wild-type and 330 bp for $Ca_V3.2$KO mice. For the *CACNA1i* gene, primers were: CACNA1iF: CTGCTGTGGTACCCTCCTGTC; CACNA1iR: GACAGGGTACCTGCTGCATG; EN-2SA-3R: GGGTTCGTGTCCTACAACAC, yielding products of 900 bp for wild-type and 545 bp for $Ca_V3.3$KO mice.[17]

Electrophysiological Recordings and Analyses

Acute horizontal brain slices (300 µm-thick) were prepared at ZT 5–6 from 3–4 week-old animals of either sex, as previously described.[17,24] In the recording chamber, slices were constantly superfused with oxygenated artificial CSF (ACSF) at 30–32°C containing (in mM): 125 NaCl, 25 $NaHCO_3$, 2.5 KCl, 1.25 NaH_2PO_4, 1.2 $MgCl_2$, 2 $CaCl_2$, 25 glucose, 1.7 L(+)-ascorbic acid. Visually identified nRt and TC neurons were whole-cell patched with borosilicate glass pipettes (TW150F-4, WPI). For recordings of passive membrane properties and spike discharges, pipettes (3–5 MΩ) were filled with an intracellular solution containing (in mM): 140 $KMeSO_4$, 10 KCl, 10 HEPES, 0.1 EGTA, 4 Mg-ATP, 0.2 Na-GTP, 10 phosphocreatine (290–300 mOsm, pH 7.25). A liquid junction potential of −10 mV was taken into account. For T-current isolation, patch pipettes (2–3 MΩ) were filled with the following solution (in mM): 135 tetramethylammonium hydroxide (TMA-OH), 40 HEPES, 10 EGTA, 2 $MgCl_2$, 4 Mg-ATP, titrated to pH 7.2 with 100 mM hydrofluoric acid (HF). The extracellular solution was supplemented with 1 µM tetrodotoxin. A liquid junction potential of −2 mV was corrected for. T-current density and activation curve were estimated as previously described.[17] For IPSC recordings in TC cells, pipettes (3–4 MΩ) were filled with (in mM): 127 CsGluconate, 10 HEPES, 2 BAPTA, 6 $MgCl_2$, 2 Mg-ATP, 0.2 Na-GTP, 10 phosphocreatine, 2.5 QX-314 (290–300 mOsm, pH 7.25). In TC neurons voltage-clamped at −30 mV, postsynaptic responses were evoked by monopolar stimulation in the internal capsule with an ACSF-filled glass electrode, in the absence of glutamatergic blockers. IPSC charge transfer was calculated as the integral of the current trace during 1s from response onset. For EPSP recordings in nRt cells, pipettes were filled with the $KMeSO_4$-based solution described above, and ACSF was supplemented with 0.1 mM picrotoxin and 0.01 mM glycine. Current-clamp recordings were conducted with automatic bridge-balance of pipette resistance. Glutamatergic afferents were electrically stimulated in the internal capsule with a paired-pulse protocol (50 ms interval). Inputs of cortical origin were selected based on the short-term facilitation of the postsynaptic responses,[25] as assessed by the ratio of the initial slopes of voltage responses to 2nd and 1st stimuli. The probability of eliciting a low-threshold spike was estimated by the presence of a burst discharge in the 2nd response (as opposed to tonic firing or lack of discharge). At least 8 paired-pulse responses were evoked in nRt cells held at −80 mV by current injections.

Series resistance (R_s) was monitored throughout recordings by brief voltage pulses, and data were rejected for R_s changes > 25%. Data were acquired through a Digidata1320 digitizer. Signals were amplified through a Multiclamp700B amplifier (Molecular Devices), sampled at 20 kHz and filtered at 10 kHz using Clampex10 (Molecular Devices). Clampfit10 (Molecular Devices) and Igor Pro 6 (WaveMetrics) were used for data analysis.

Chemicals

All standard salts and chemicals were purchased from SigmaAldrich, except the following: $KMeSO_4$ (ICN Biomedicals); L(+)-ascorbic acid (VWR Prolabo); Tetrodotoxin, (Latoxan); QX-314-Cl (Alomone Labs), picrotoxin (Abcam).

Polysomnographic Recordings and Analyses

Electroencephalographic (EEG/ECoG) and electromyographic (EMG) recordings were performed in male $Ca_V3.2$KO mice, Ca_V3.DKO mice and wild-type mice chronically implanted with electrodes for differential fronto-parietal EEG and nuchal muscle EMG, as previously described.[17,26] EEG electrodes were 2 gold-plated screws (1.1 mm diameter) implanted on the right hemisphere ~1.5 mm frontal to the bregma and ~1.5 mm frontal to the lambda, respectively, both at ~1.5 mm from the central fissure. Four further screws were inserted on the 2 hemispheres at symmetrical positions to stabilize the pin connector. EMG electrodes were gold wires with a diameter of 0.2 mm. The whole implant was fixed to the skull with a first layer of resin cement (RelyX, 3-M, or G-CEM, GC America Inc.) and then covered with Paladur (Heraeus Kulzer). At the time of surgery, animals were 6–9 weeks old. Ca_V3.DKO mice had slightly lower body weights (wild-type: 22.3 ± 0.9 g, n = 8 vs. $Ca_V3.2$KO: 21.8 ± 0.7 g, n = 8, and Ca_V3.DKO: 19.3 ± 0.9 g, n = 8; P = 0.058, one-way ANOVA). During one week of post-surgery recovery, mice received paracetamol (2 mg/mL) in drinking water. Animals were allowed one additional week to habituate once electrode implants were connected to the tethering cables. Polysomnographic acquisitions were performed in 48 h-long sessions with groups of 4 animals. The analog EEG and EMG signals were first amplified (gain 2000 x), and then high-pass filtered at 0.7 Hz and 10 Hz, respectively. Data were digitized at 2 kHz and down-sampled to 200 Hz through Somnologica 3.3.1 software (Embla System). Vigilance states were visually scored as wakefulness, NREM or REM sleep based on EEG/EMG signals according to well-established criteria.[26] Power spectra were determined from 48-h long recordings using discrete-Fourier transformation between 0.75 to 90 Hz (0.25 Hz bins) for consecutive 4-s epochs. For spectral analysis, a given epoch was rejected when an adjacent epoch was scored to a different vigilance state or contained movement artifacts. On average, 74% ± 5% of the total waking time, 93% ± 1% of the total NREM sleep time and 75% ± 2% of the total REM sleep time were included in the spectral analysis of wild-type animals. The corresponding values for $Ca_V3.2$KO mice are 82% ± 6%, 94% ± 1%, 84% ± 1%, and, for Ca_V3.DKO mice, 74% ± 7%, 91% ± 1% and 76% ± 4%. Mean power spectra were calculated as the average of all artifact-free 4-s epochs of the corresponding vigilance state during both light and dark phase. Sigma power at NREM-to-REM sleep transition was determined according to previously described procedures,[3,26] with % σ power expressed relative to the mean values at min 0.5–1.5 after the transition to REM sleep. Microarousals were defined as waking episodes of ≤ 16 s duration preceded and followed by at ≥ 5 and ≥ 4 NREM sleep episodes, respectively. EEG analyses were performed with customized semi-automated routines written in Matlab v8.5 R2015a (The Mathworks).

Statistical Analyses

Data are presented as mean ± SEM, with "n" indicating the number of cells for *in vitro* recordings, and number of animals for EEG datasets. The use of parametric or nonparametric statistical tests was based on the normal distribution of the data. One-way ANOVA and repeated measures ANOVA were performed in JMP.10 (SAS Institute Inc.), followed by post hoc Student *t*-test, with significance accepted for $\alpha < 0.05$. Greenhouse-Geisser (G-G) correction was applied to account for violation of sphericity (Mauchly test), where necessary. Cumulative distributions of bouts of behavioral states were compared with the Kolmogorov-Smirnov test in Matlab, with a significance level of 0.01.

RESULTS

Abolishment of nRt Low-Threshold Burst Discharges in Ca_V3.DKO Mice

In acute brain slices from wild-type, $Ca_V3.2$KO and Ca_V3.DKO mice, we compared basic electrophysiological parameters of nRt neurons by means of whole-cell patch-clamp recordings (Figure 1). No overt difference between genotypes was present for values of resting membrane potential (V_{rmp}: wild-type, −64.6 ± 2.6 mV; $Ca_V3.2$KO, −67.9 ± 2.6 mV; Ca_V3.DKO, −70.9 ± 3.1 mV), cell capacitance (C_m: wild-type, 78.7 ± 7 pF; $Ca_V3.2$KO, 85.9 ± 10 pF; Ca_V3.DKO, 80.0 ± 5 pF), and input resistance (R_i: wild-type, 204.8 ± 31.4 MΩ; $Ca_V3.2$KO, 207.4 ± 34.2 MΩ; Ca_V3.DKO, 227.5 ± 24.9 MΩ) (wild-type, n = 11 cells; $Ca_V3.2$KO, n = 9; Ca_V3.DKO, n = 9; for all parameters P > 0.05, one-way ANOVA; Figure 1A). Current responses to hyperpolarizing voltage steps, which include activation of inwardly rectifying and HCN channels, were also comparable (Figure 1B). Moreover, tonic firing elicited by depolarizing current injections (400 ms) from a holding potential of −70 mV displayed similar input-output relationships (wild-type, n = 9; $Ca_V3.2$KO, n = 8; Ca_V3.DKO, n = 9; Figure 1C). We noticed a tendency of Ca_V3.DKO neurons to sustain prolonged tonic firing, whereas wild-type and $Ca_V3.2$KO often displayed strong accommodation after the first 200 ms of depolarization. We quantified spiking frequency during the second half of the 400 ms-long depolarization, and found a consistent tendency for an increase in Ca_V3.DKO neuron firing rate (e.g. 400 pA step: wild-type, 26.7 ± 17.8 Hz; $Ca_V3.2$KO, 26.8 ± 10.1 Hz; Ca_V3.DKO, 43.9 ± 11.7 Hz; P > 0.05). This is consistent with a previous study reporting on increased propensity of Ca_V3.DKO nRt cells to generate tonic firing during prolonged step depolarization (> 1 s).[27]

We next examined low-threshold spiking generated at the offset of brief hyperpolarizing current steps (Figure 2). Wild-type cells (n = 10) displayed rhythmic low-threshold Ca^{2+} spikes accompanied by bursts of Na^+ action potentials, the number of which varied depending on the initial membrane potential. Typically, bursts discharges were best elicited at V_m values in the range between −70 mV and −55 mV. Interestingly, in nRt cells from $Ca_V3.2$KO mice, no significant change in repetitive bursting was found (P > 0.05; n = 9; Figure 2C, 2D). Inter-burst intervals measured for discharges elicited from −70 mV also did not differ between genotypes (interval between initial APs of the first and second burst: wild-type, 168 ± 16 ms, n = 6; $Ca_V3.2$KO, 181 ± 14 ms, n = 8; P > 0.05, unpaired *t*-test). By contrast, Ca_V3.DKO mice displayed a complete lack of oscillatory low-threshold spiking, as previously reported.[27] Occasionally, a single action potential appeared in Ca_V3.DKO cells at

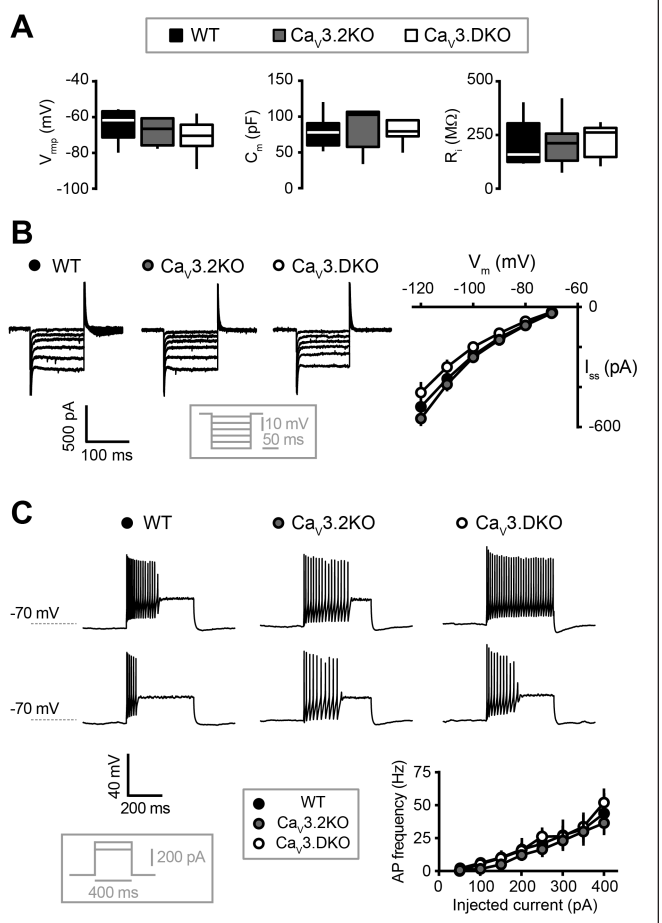

Figure 1—Lack of overt changes in passive properties and tonic discharge of nRt cells of $Ca_V3.2KO$ and $Ca_V3.DKO$ mice. **(A)** Box-and-whisker plots with values of resting membrane potential (V_{rmp}), membrane capacitance (C_m) and input resistance (R_i) of nRt cells from wild-type (WT, n = 11), $Ca_V3.2KO$ (n = 9) and $Ca_V3.DKO$ (n = 9) mice. The midline in each box represents the median, the whiskers are 10th and 90th percentiles. **(B)** Left, representative current responses to hyperpolarizing voltage steps from −60 mV for all genotypes. Inset: protocol. Right, steady-state current (I_{ss}) for WT (n = 10), $Ca_V3.2KO$ (n = 9) and $Ca_V3.DKO$ (n = 9) nRt cells over a range of voltages. **(C)** Top, representative tonic discharges in WT, $Ca_V3.2KO$ and $Ca_V3.DKO$ nRt cells elicited by positive current injections from −70 mV. Bottom, average discharge frequency of tonic action potentials (APs) during the 400 ms over a range of positive currents injected (WT, n = 9; $Ca_V3.2KO$, n = 8; $Ca_V3.DKO$, n = 9; P > 0.05). Inset: current-clamp protocol.

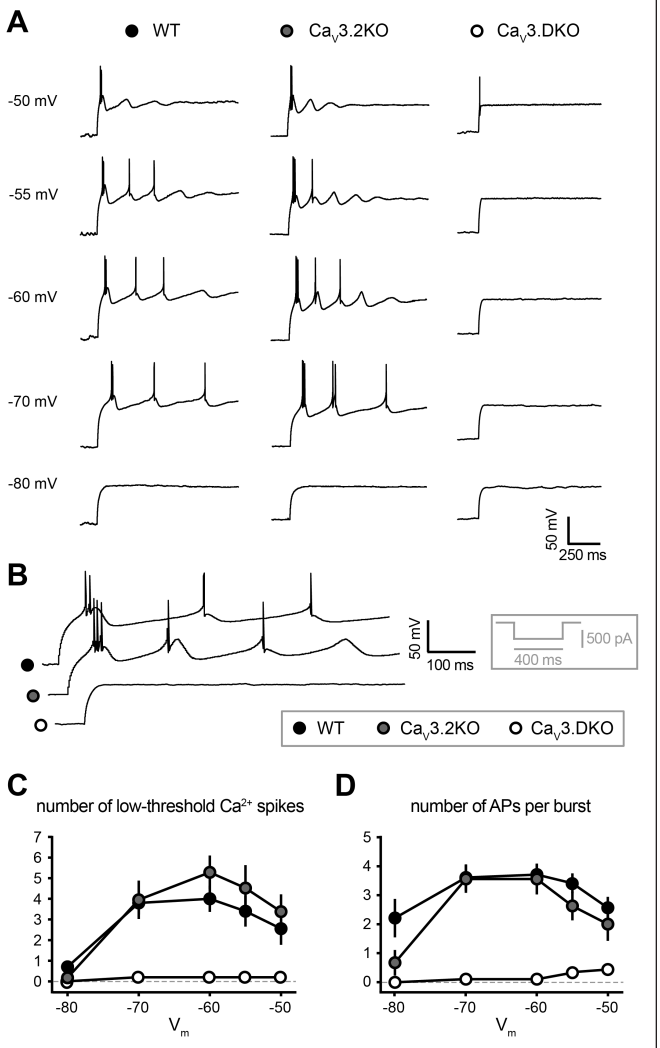

Figure 2—Suppression of oscillatory low-threshold bursting in nRt cells from $Ca_V3.DKO$ mice. **(A)** Representative traces of low-threshold bursting in WT, $Ca_V3.2KO$ and $Ca_V3.DKO$ nRt cells elicited at the offset of negative current injections from different membrane potentials, as indicated. **(B)** Expanded traces from **(A)** at −60 mV. Inset: current-clamp protocol. **(C)** Number of low-threshold Ca^{2+} spikes and **(D)** number of action potentials (APs) during the first burst in WT (n = 10), $Ca_V3.2KO$ (n = 9), and $Ca_V3.DKO$ (n = 9) mice.

the offset of hyperpolarizing steps applied from more depolarized membrane potentials (−50 mV, observed in 4 of 9 cells).

Next, we quantified the contribution of $Ca_V3.2$ channels to isolated low-threshold Ca^{2+} currents (T-currents) that were elicited by increasing depolarizing steps applied to nRt cells voltage-clamped at −100 mV (Figure 3). Compared to wild-type cells, currents from $Ca_V3.2KO$ cells displayed a slight prolongation of inactivation kinetics ($\tau_{w,\ decay}$ at −60 mV: wild-type, 58.9 ± 4.5 ms, n = 9; $Ca_V3.2KO$, 83.1 ± 10.9 ms, n = 8; P = 0.07, unpaired *t*-test; Figure 3A), consistent with previous data from younger (2 week-old) $Ca_V3.2KO$ mice.[18] Activation kinetics were equivalent (10% to 90% rise time at −60 mV: wild-type, 6.8 ± 0.6 ms, n = 9; $Ca_V3.2KO$, 6.1 ± 0.5 ms, n = 8; P > 0.05, unpaired *t*-test; Figure 3A). Current density and activation curve were comparable, with no significant modification in the estimated V_{half} (wild-type, −71.1 ± 1.0 mV, n = 9; $Ca_V3.2KO$, −69.8 ± 1.7 mV, n = 8; P > 0.05, unpaired *t*-test; Figure 3B). In $Ca_V3.DKO$ mice, no detectable T-currents were generated across the entire range of voltage steps (n = 9).

Together, deletion of $Ca_V3.2$ and $Ca_V3.3$ channels completely abolished T-currents in nRt cells, with a consequent suppression of repetitive oscillatory low-threshold discharges. The absence of the $Ca_V3.2$ subtype did not induce overt changes in the single-cell electrophysiological profile, confirming the dominant role of $Ca_V3.3$ channels in setting nRt cells responsiveness to somatic voltage fluctuations.[17] However, it is also well known that the electrotonic properties of the thin nRt cell

dendrites hamper proper space-clamp, which prevents the controlled activation of voltage-dependent conductances in distal compartments.[28] This could be one reason for which a $Ca_V3.2$-current component went undetected in our somatic whole-cell recordings.

Impaired Intrathalamic GABAergic Transmission in Ca_V3.DKO Mice

We next examined the impact of $Ca_V3.2$ and $Ca_V3.3$ channel deletion on synaptic transmission and excitability within intrathalamic networks, which are both relevant for sleep rhythm generation.[17,29] We first verified whether thalamocortical (TC) cells in the ventrobasal nucleus (VB) continue to generate low-threshold discharges via $Ca_V3.1$ channels[13,14] when their synaptic partners in the nRt are burst-deficient. TC cells from wild-type, $Ca_V3.2$KO and Ca_V3.DKO mice displayed comparable responses to hyperpolarizing current injections, which reliably elicited low-threshold spikes crowned by the same number of action potentials (number of APs in bursts generated by a current injection of −250 pA: wild-type, 2.8 ± 0.4, n = 9; $Ca_V3.2$KO, 2.5 ± 0.5, n = 6; Ca_V3.DKO, 2.2 ± 0.4, n = 6; $P > 0.05$, one-way ANOVA; Figure 4A).

Low-threshold bursting of nRt generates phasic inhibitory currents in TC cells comprising a fast and a slow component, mediated by synaptic and non-synaptic $GABA_A$ receptors, respectively.[29,30] In TC cells held at −30 mV using low Cl^--based electrodes we evoked IPSCs by electrically stimulating the internal capsule, while leaving excitatory transmission intact, thus permitting the recruitment of nRt cell discharges by glutamatergic inputs. In wild-type mice, evoked responses in TC cells typically consisted of multiphasic "burst IPSCs" (bIPSCs) at stimulation intensities > 100 μA, with a sequence of fast events riding on a slower current envelope, previously reported to result from presynaptic burst discharge.[17,29,31] Deletion of $Ca_V3.2$ channels decreased the charge transfer of bIPSCs elicited at higher intensities (250–300 μA: wild-type, 91.0 ± 21.1 pC, n = 7; $Ca_V3.2$KO, 50.7 ± 10.7 pC, n = 8; $P < 0.05$ one-way ANOVA; Figure 4B). By contrast, in TC cells from Ca_V3.DKO, only small monophasic IPSCs lacking the waveform typical for bIPSCs could be evoked, and the charge transfer was strongly diminished (250–300 μA: Ca_V3.DKO, 13.5 ± 3.6 pC, n = 7; $P < 0.01$ compared to wild-type; Figure 4B). Finally, we examined the responsiveness of nRt cells to cortical glutamatergic inputs, which are thought to initiate spindle rhythmogenesis by activating low-threshold conductances in nRt dendrites.[32,33] In current-clamped nRt cells at −80 mV, we evoked EPSPs of cortical origin by selecting responses that exhibited short-term facilitation upon paired-pulse stimulation in the internal capsule.[25] Paired-pulse ratio of the initial slope of voltage responses was comparable between genotypes (wild-type, 2.2 ± 0.2, n = 8; $Ca_V3.2$KO, 2.4 ± 0.2, n = 7; Ca_V3.DKO, 2.7 ± 0.4, n = 6; $P > 0.05$ one-way ANOVA; Figure 4C). In wild-type and in $Ca_V3.2$KO mice, the second stimulus typically elicited a low-threshold burst, with an occurrence of 68% ± 8% and 52% ± 15%, respectively. In Ca_V3.DKO mice, no bursting was generated ($P < 0.01$ Wilcoxon test, compared to the other genotypes), despite the sufficient depolarization provided by the second stimulus (on average 12.5 ± 1.2 mV), which occasionally elicited a single suprathreshold action potential (in 2 of 6 cells).

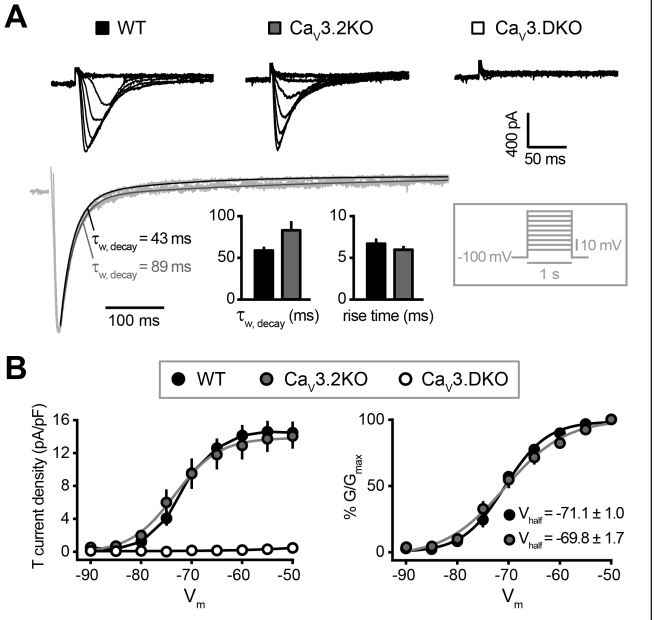

Figure 3—Elimination of low-threshold Ca^{2+} currents in nRt cells from Ca_V3.DKO mice. **(A)** Top, isolated low-threshold Ca^{2+} currents elicited by depolarizing steps from −100 mV in WT, $Ca_V3.2$KO and Ca_V3.DKO nRt cells. Bottom, representative traces scaled to peak and bar graphs showing mean values for decay time constant ($\tau_{w, decay}$) and rise time (10% to 90%) from WT and $Ca_V3.2$KO (WT, n = 9; $Ca_V3.2$KO, n = 8; $P > 0.05$). Inset: voltage-clamp protocol. **(B)** T-current density for all genotypes (left) and activation curve (right) of the T-currents for WT and $Ca_V3.2$KO with estimated V_{half} (WT: −71.1 ± 1.0 mV, n = 9; $Ca_V3.2$KO: −69.8 ± 1.7 mV, n = 8; $P > 0.05$). In Ca_V3.DKO mice, no detectable T-currents were generated across the whole range of voltage steps (n = 9).

Together, these data reveal a pronounced deficit in the intrathalamic GABAergic transmission in Ca_V3.DKO mice, which is due to an impaired capability of nRt in generating low-threshold discharges. Although the deletion of $Ca_V3.2$ channels did not appear to affect nRt repetitive bursts in response to somatic current injections, $Ca_V3.2$KO mice displayed a reduction in the charge transfer of bIPSCs. This discrepancy between somatically and synaptically elicited bursting suggests that $Ca_V3.2$ deletion affects the efficacy of excitatory inputs in recruiting nRt dendritic Ca^{2+} conductances.

EEG Sleep Profile of $Ca_V3.2$KO and Ca_V3.DKO Mice

The lack of low-threshold bursting in nRt cells from Ca_V3.DKO mice predicted a marked deregulation of thalamic sleep rhythmogenesis. In particular, we expected Ca_V3.DKO mice to exhibit deficits in sleep spindle generation, which depends on nRt bursting and on reverberatory activity within the nRt-TC loop.[32,34,35] We performed polysomnographic recordings in freely behaving wild-type (n = 8), $Ca_V3.2$KO mice (n = 8), and Ca_V3.DKO mice (n = 8) chronically implanted with EEG/EMG electrodes and recorded under undisturbed conditions for 48 h. In the following, we describe sleep architecture and EEG power spectra during NREM sleep, REM sleep, and waking in the three genotypes.

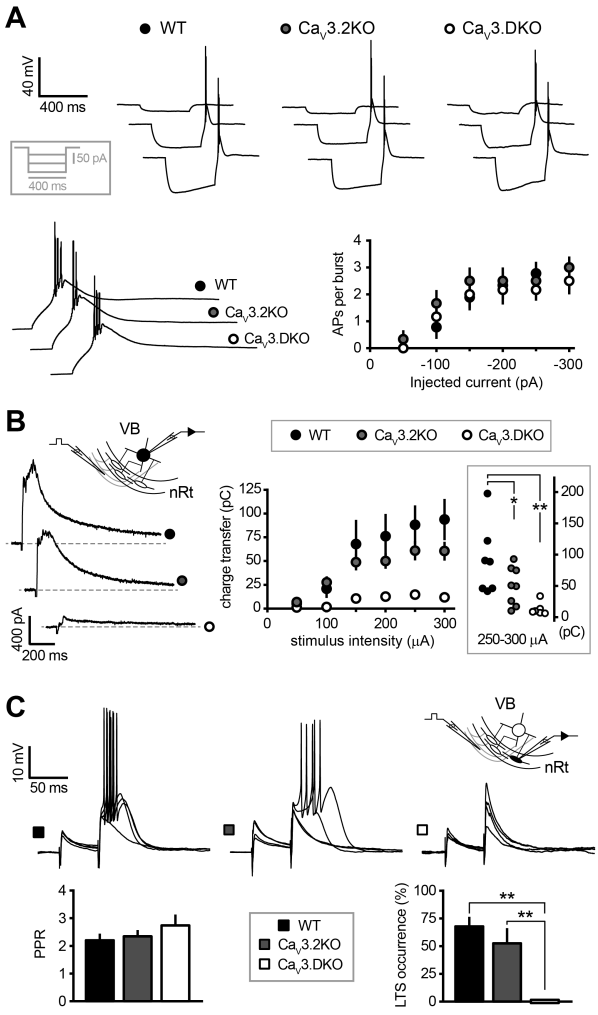

Figure 4—Consequences of $Ca_V3.2$ and $Ca_V3.3$ channel deletion for nRt-TC GABAergic transmission. **(A)** Top, representative traces of rebound bursting elicited by hyperpolarizing current injections discharges in TC neurons held at −70 mV. Inset: current-clamp protocol. Bottom left, expanded traces shown in **(A)** for a −150 pA step of current injection. Bottom right, the number of action potentials per burst across a range of injected current did not change between genotypes (WT, n = 9, $Ca_V3.2$KO, n = 6, $Ca_V3.3$DKO, n = 6; P > 0.05). **(B)** Left, example traces of evoked IPSCs recorded in TC cells at −30 mV upon electrical stimulation in the internal capsule. Inset, recording configuration showing site of stimulation in the internal capsule while recording from a TC cell in the ventrobasal nucleus (VB). Right, charge transfer across a range of stimulus intensities for all genotypes showing a minor and a strong decrease in the $Ca_V3.2$KO and $Ca_V3.3$DKO mice, respectively, compared to WT animals. Inset shows mean responses to higher stimulus intensities (250–300 μA) (WT, n = 7, $Ca_V3.2$KO, n = 8; $Ca_V3.3$DKO, n = 7; one-way ANOVA, P < 0.05; **P < 0.01, *P < 0.05, post hoc unpaired *t*-test). **(C)** Top, examples of postsynaptic responses evoked in nRt cells at −80 mV upon stimulation of cortical afferents. Inset, recording configuration showing stimulation site in the internal capsule. Paired-pulse stimuli (50 ms interval) were delivered to select for responses of cortical origin based on short-term facilitation. Bottom, bar graphs showing mean values of paired-pulse ratio (PPR), measured from the initial slope of voltage responses, and occurrence of low-threshold spiking (LTS) on the second stimulus (WT, n = 8, $Ca_V3.2$KO, n = 7; $Ca_V3.3$DKO, n = 6; one-way ANOVA, P > 0.05 for PPR and Wilcoxon test, P < 0.05 for LTS occurrence; **P < 0.01 nonparametric multiple comparison).

$Ca_V3.2$KO mice spent similar amounts of time in the different vigilance states as compared to wild-type animals, except for a slight reduction in NREM sleep during the dark phase ($F_{2.0,\ 21.3}$ = 2.8, P = 0.08; Figure 5A). During the light phase, $Ca_V3.3$DKO mice spent, on average, more time in NREM sleep and less time in waking, as compared to wild-type and $Ca_V3.2$KO mice ($F_{2.4,\ 25.3}$ = 6.6, P < 0.01). Inspection of sleep bout length revealed that NREM sleep episodes of long duration (> 252 s) occurred more frequently in $Ca_V3.2$KO mice, whereas bouts of intermediate duration (32–252 s) were predominant in $Ca_V3.3$DKO mice at the expense of long episodes ($F_{2.0,\ 21.3}$ = 12.3, P < 0.01; Figure 5B). By contrast, no alterations were found in episode length and global time spent in REM sleep ($F_{2.6,\ 27.2}$ = 2.3, P > 0.05; Figure 5A, 5B) or in the number of transitions from NREM to REM sleep (per hour of NREM sleep: 6.0 ± 0.5 in wild-type vs. 6.7 ± 0.4 in $Ca_V3.2$KO mice, and 5.8 ± 0.4 in $Ca_V3.3$DKO mice, P > 0.05). The changes in NREM sleep architecture appeared to be counterbalanced by alterations in waking episodes. Compared to wild-type and $Ca_V3.2$KO mice, $Ca_V3.3$DKO mice spent more time in brief and intermediate periods of wakefulness (< 32 s, 32–124 s, $F_{2.1,\ 22.5}$ = 11.6, P < 0.01; Figure 6A), and, interestingly, NREM sleep episodes were more frequently interrupted by microarousals (per hour of NREM sleep: 13.2 ± 1.1 microarousals in wild-type vs. 8.8 ± 0.9 in $Ca_V3.2$KO mice, and 17.6 ± 0.9 in $Ca_V3.3$DKO mice, P < 0.01 for both KO genotypes compared to wild-type). Thus, although $Ca_V3.3$DKO mice spent globally more time in NREM sleep episodes, these were of shorter duration, and sleep was generally more disrupted by short awakenings.

Next, we examined EEG power spectra of NREM and REM sleep. Absolute values of NREM sleep EEG power did not significantly differ between genotypes, although $Ca_V3.3$DKO mice appeared to show an increase in the low-frequency range (slow-wave activity, SWA, 0.75–4 Hz) during both light and dark phase (Figure 5C).

To examine the relative contribution of specific spectral frequencies to the global EEG profile, and to account for inter-individual variations in EEG signal amplitude, we compared percentage EEG power values obtained by normalizing each frequency bin to the total power for each behavioral state (Figure 5D). Whereas wild-type and $Ca_V3.2$KO mice had largely superimposable NREM sleep power spectra, significant differences were visible in $Ca_V3.3$DKO mice ($F_{2.7,\ 27.9}$ = 4.5, P < 0.05). In particular, a marked reduction occurred across the whole σ frequency range (10–15 Hz: 0.57% ± 0.03% in wild-type vs. 0.56% ± 0.03% in $Ca_V3.2$KO mice, and 0.41% ± 0.01% in $Ca_V3.3$DKO mice; P < 0.01, post hoc unpaired *t*-test). A compromised spindle rhythmogenesis in $Ca_V3.3$DKO mice was also found when EEG power dynamics were analyzed at transitions between NREM and REM sleep, which are spindle-rich periods.[17,26] In the NREM sleep epochs preceding REM sleep, σ power typically exhibits a surge, which is accompanied by a decrease in δ power, indicative of reduced sleep depth. $Ca_V3.2$KO mice displayed a partially reduced σ power surge, which, in $Ca_V3.3$DKO mice, was further diminished (570 ± 43% in wild-type vs. 438 ± 15% in $Ca_V3.3$DKO mice and 328 ± 15% in $Ca_V3.3$DKO mice; P < 0.01, Figure 5E) and also preceded by a lower level of basal σ power. In contrast to the changes

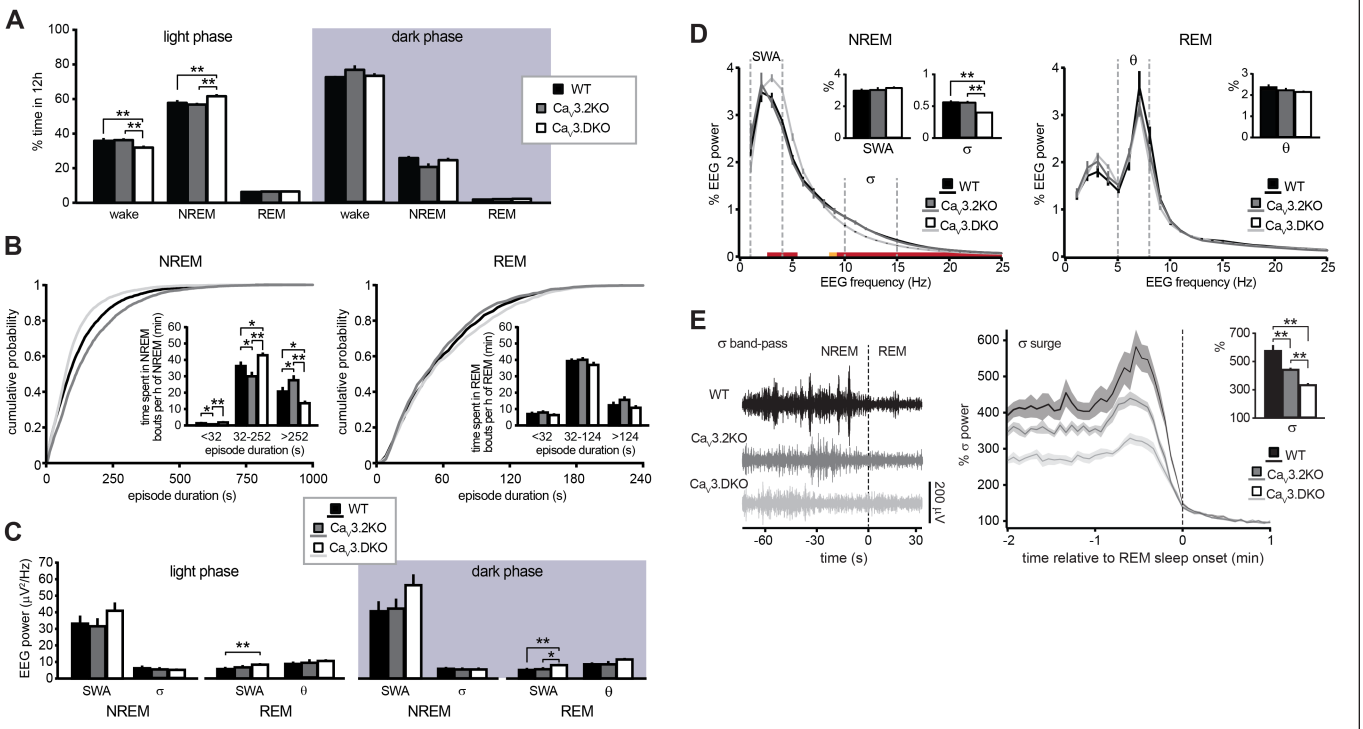

Figure 5—Comparison of the EEG sleep profile of WT, $Ca_V3.2$KO, and Ca_V3.DKO mice. **(A)** Time spent in wake, NREM and REM sleep, expressed in % of 12 h and separated for light and dark period, for WT (n = 8), $Ca_V3.2$KO (n = 8), and Ca_V3.DKO (n = 8) mice. During the light phase, Ca_V3.DKO showed an increased amount of NREM sleep, while waking was reduced (state × genotype interaction: $F_{2.4, 25.3} = 6.6$, $P < 0.05$; **$P < 0.01$, post hoc unpaired *t*-test). No change occurred during the dark phase ($F_{2.0, 21.3} = 2.8$, $P > 0.05$). **(B)** Cumulative distributions of NREM and REM sleep episode duration pooled for light and dark phase. Statistical significance was tested with K-S statistics ($P < 0.01$ between all genotypes for NREM sleep). Insets, histograms of time spent in short, intermediate and long episodes per hour of corresponding sleep (duration × genotype interaction: $F_{2.0, 21.3} = 12.3$, $P < 0.01$ for NREM sleep and $F_{2.6, 27.2} = 2.3$, $P > 0.05$ for REM sleep; *$P < 0.05$, **$P < 0.01$, post hoc unpaired *t*-test). **(C)** Mean absolute power of relevant frequency bands during NREM or REM sleep separated for light and dark phase (SWA (0.75–4 Hz), σ (10–15 Hz), and θ (5–8 Hz); one-way ANOVA, $P < 0.05$ and $P < 0.01$ for SWA of light and dark phase, respectively; *$P < 0.05$, **$P < 0.01$, post hoc unpaired *t*-test). **(D)** Normalized EEG power spectrum between 0.75 and 25 Hz for NREM (left) and REM (right) sleep. Red and orange lines on the x axes delineate intervals of frequency for Ca_V3.DKO mice with a significant difference compared to WT and $Ca_V3.2$KO mice, with $P < 0.01$ and $P < 0.05$, respectively, tested with post hoc unpaired *t*-test after repeated measures ANOVA (genotype × frequency interaction: $F_{2.7, 27.9} = 4.5$, $P < 0.05$ for NREM sleep and $F_{3.2, 33.4} = 1.8$, $P > 0.05$ for REM sleep). Dotted lines indicate frequency ranges for SWA (0.75–4 Hz), σ (10–15 Hz), and θ (5–8 Hz) bands used for the mean values presented in the bar graphs in the insets (one-way ANOVA, $P < 0.05$ for σ; **$P < 0.01$, post hoc unpaired *t*-test). **(E)** Left, examples of σ band-pass-filtered EEG recordings containing NREM-to-REM sleep transitions (occurring at time zero). Right, time course of mean EEG power in the σ band at NREM-to-REM sleep transitions in WT (n = 8), $Ca_V3.2$KO (n = 8), and Ca_V3.DKO (n = 8) mice during light and dark phase. Data were normalized to the mean power from 0.5 to 1.5 min after the transition to REM sleep. Shaded areas represent SEM. The dashed line at zero indicates REM sleep onset. Bar graph represents peak values of % σ power before REM sleep onset (one-way ANOVA, $P < 0.01$; **$P < 0.01$, post hoc unpaired *t*-test).

in σ power, relative EEG power in the low-frequency range was globally unaltered (0.75–4 Hz: 3.0% ± 0.1% in wild-type vs. 3.0% ± 0.2% in Ca_V3.DKO mice and 3.2% ± 0.1% in Ca_V3.DKO mice; $P > 0.05$, post hoc unpaired *t*-test). Interestingly, however, in Ca_V3.DKO mice a significant increase was obtained when the higher range of δ frequencies was considered (2–4 Hz: 3.2 ± 0.1% in wild-type vs. 3.2 ± 0.1% in $Ca_V3.2$KO mice and 3.6 ± 0.1% in Ca_V3.DKO mice, $P < 0.05$ for Ca_V3.DKO mice compared to wild-type and $Ca_V3.2$KO; post hoc unpaired *t*-test).

The normalized EEG power spectrum of REM sleep was not significantly altered in $Ca_V3.2$KO and Ca_V3.DKO mice ($F_{3.2, 33.4} = 1.8$, $P > 0.05$; Figure 5D). A slight increase in the higher range of δ frequencies during REM sleep seemed to gradually appear with *Ca_V3* single and double deletion (2–4 Hz: 1.70% ± 0.11% in wild-type vs. 1.86% ± 0.13% in $Ca_V3.2$KO mice and 1.93% ± 0.03% in Ca_V3.DKO mice; $P > 0.05$). A difference in SWA was visible for absolute values of REM sleep EEG power of Ca_V3.DKO mice ($P < 0.01$ compared to wild-type, for both phases; Figure 5C).

Absolute values of waking EEG power of Ca_V3.DKO mice exhibited a general increase across frequency bands during both light and dark phase compared to wild-type and $Ca_V3.2$KO mice ($P < 0.01$ for both phases; Figure 6B). The relative contribution of the distinct frequency bands to the normalized power spectra was different ($F_{5.6, 59.5} = 3.48$, $P < 0.01$), in particular at frequency ranges corresponding to the α (8–12 Hz) and the β (12–20 Hz) band that displayed, on average, a significant reduction (8–12 Hz and 12–20 Hz: 0.89% ± 0.05% and 0.29% ± 0.01% in wild-type vs. 0.94% ± 0.05% and 0.28% ± 0.01% in $Ca_V3.2$KO mice, and 0.70% ± 0.02% and 0.25% ± 0.01% in Ca_V3.DKO mice, $P < 0.01$ for Ca_V3.DKO

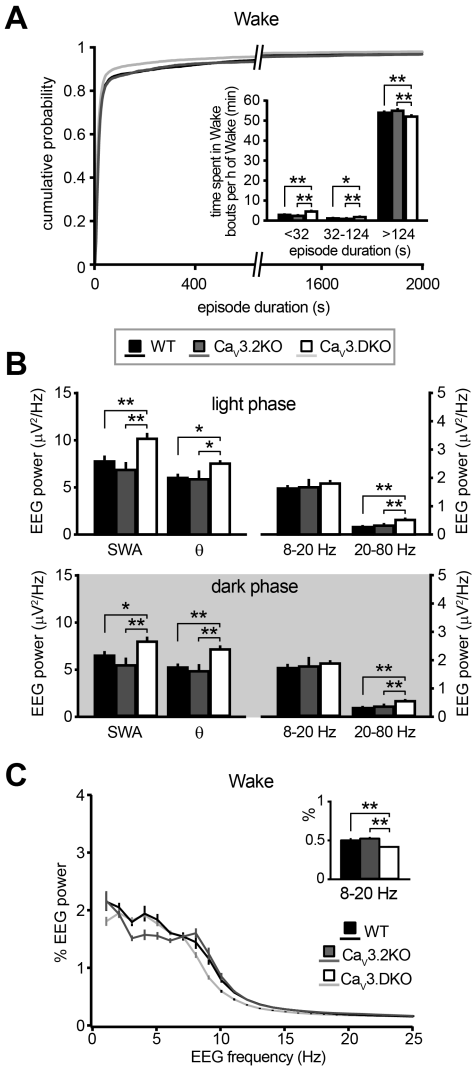

Figure 6—Comparison of wake EEG profile of wild-type, $Ca_V3.2$KO, and Ca_V3.DKO mice. **(A)** Cumulative distributions of wake episode durations during both light and dark phase. Statistical significance was tested with K-S statistics (P < 0.01 between all genotypes). Inset, histogram showing time spent in short, intermediate and long episodes per hour of wake (duration × genotype: $F_{2.1, 22.5} = 11.6$, P < 0.01; *P < 0.05, **P < 0.01, post hoc unpaired *t*-test). **(B)** Mean absolute power of relevant frequency bands separated for light and dark phase (SWA (0.75–4 Hz), θ (5–8 Hz); *P < 0.05, **P < 0.01, post hoc unpaired *t*-test after one-way ANOVA). **(C)** Normalized EEG spectral power between 0.75 and 25 Hz during waking (genotype × frequency interaction: $F_{5.6, 59.5} = 3.48$, P < 0.01). Inset, mean values of normalized EEG power in the frequency range 8–20 Hz for WT, $Ca_V3.2$KO, and Ca_V3.DKO (one-way ANOVA, P < 0.01; **P < 0.01, post hoc unpaired *t*-test).

mice compared to wild-type and $Ca_V3.2$KO, post hoc unpaired *t*-test; Figure 6C).

Altogether, analysis of sleep EEG power indicates distinct contributions of $Ca_V3.2$ and $Ca_V3.3$ channels to thalamocortical rhythmogenesis. *$Ca_V3.2$* single deletion did not cause major alterations to the spectral profile of NREM sleep. However, some differences in σ power dynamics were observed at transitions between NREM and REM sleep, i.e., at periods of enhanced sleep spindle rhythmogenesis. *$Ca_V3.2$* and *$Ca_V3.3$* double deletion induced a marked decrease in the relative contribution of the σ frequency range that was also evident in the average NREM sleep power spectrum, consistent with a constitutive impairment in sleep spindle rhythmogenesis. Additionally, the EEG power in the δ frequency range was augmented. Ca_V3.DKO mice spent more time in NREM sleep, but the predominance of short NREM sleep episodes together with the increase in microarousals indicates a more fragmented sleep architecture.

DISCUSSION

This work contributes to clarify the roles of Ca^{2+} channels for thalamic oscillations and sleep rhythms. In line with previous results, our data provide further evidence for a dominant role of $Ca_V3.3$ subtype in sustaining nRt low-threshold bursting and in activating the intrathalamic loop that underlies spindle pacemaking. In addition, our findings point at a modulatory function of the $Ca_V3.2$ subtype for nRt excitability, which might be involved in dynamically changing the strength of thalamic oscillations, e.g., by boosting sleep spindle rhythmogenesis at NREM to REM transitions. Based on these observations, we propose that the co-expression of $Ca_V3.2$ and $Ca_V3.3$ subtypes in nRt underlies distinct aspects of this pacemaker structure in rhythmogenesis. In addition, the lack of low-threshold Ca^{2+} currents in Ca_V3.DKO mice excludes a functional contribution of the $Ca_V3.1$ subtype, although molecular analyses have also identified the presence of this isoform in nRt cells.[36]

Our study was largely based on a comparative analysis of single KOs for $Ca_V3.2$ channels and the DKO lacking both $Ca_V3.2$ and $Ca_V3.3$ channels (Figure 7). We found that removal of $Ca_V3.2$ channels alone did not cause major alterations to nRt discharge, consistent with previous reports indicating a major contribution of $Ca_V3.3$ channels.[17,18] In particular, low-threshold oscillatory bursting typical for NREM sleep rhythms, such as sleep spindles, was largely preserved in $Ca_V3.2$KO mice, and the underlying T-currents were comparable with wild-type levels.

We have analyzed cell excitability by applying somatic voltage steps, which might amplify the activation of proximal Ca_V3 channels and underestimate the contribution of distal compartments, especially in the case of the elongated dendrites of nRt neurons.[37] Are $Ca_V3.2$ channels preferentially located in distal dendritic branches? T-currents in nucleated patches from younger mice were shown to display higher Ni^{2+} sensitivity and faster inactivation kinetics than whole-cell T-currents, indicating that, at least during development, $Ca_V3.2$ channels are mainly located at proximal sites.[28]

We have further characterized the capability of Ca_V3 channels to generate nRt discharge when synaptically recruited. Upon stimulation of glutamatergic inputs onto nRt, bIPSCs could still be evoked in TC cells of $Ca_V3.2$KO mice, although with a reduced charge transfer, whereas this form of GABAergic transmission was impaired by *$Ca_V3.3$* ablation.[17] Synaptic recruitment of $Ca_V3.3$ channels is hence obligatory for bIPSC generation, whereas $Ca_V3.2$ channels additionally appear to boost synaptic transmission mediated through burst discharge. A modulatory function for

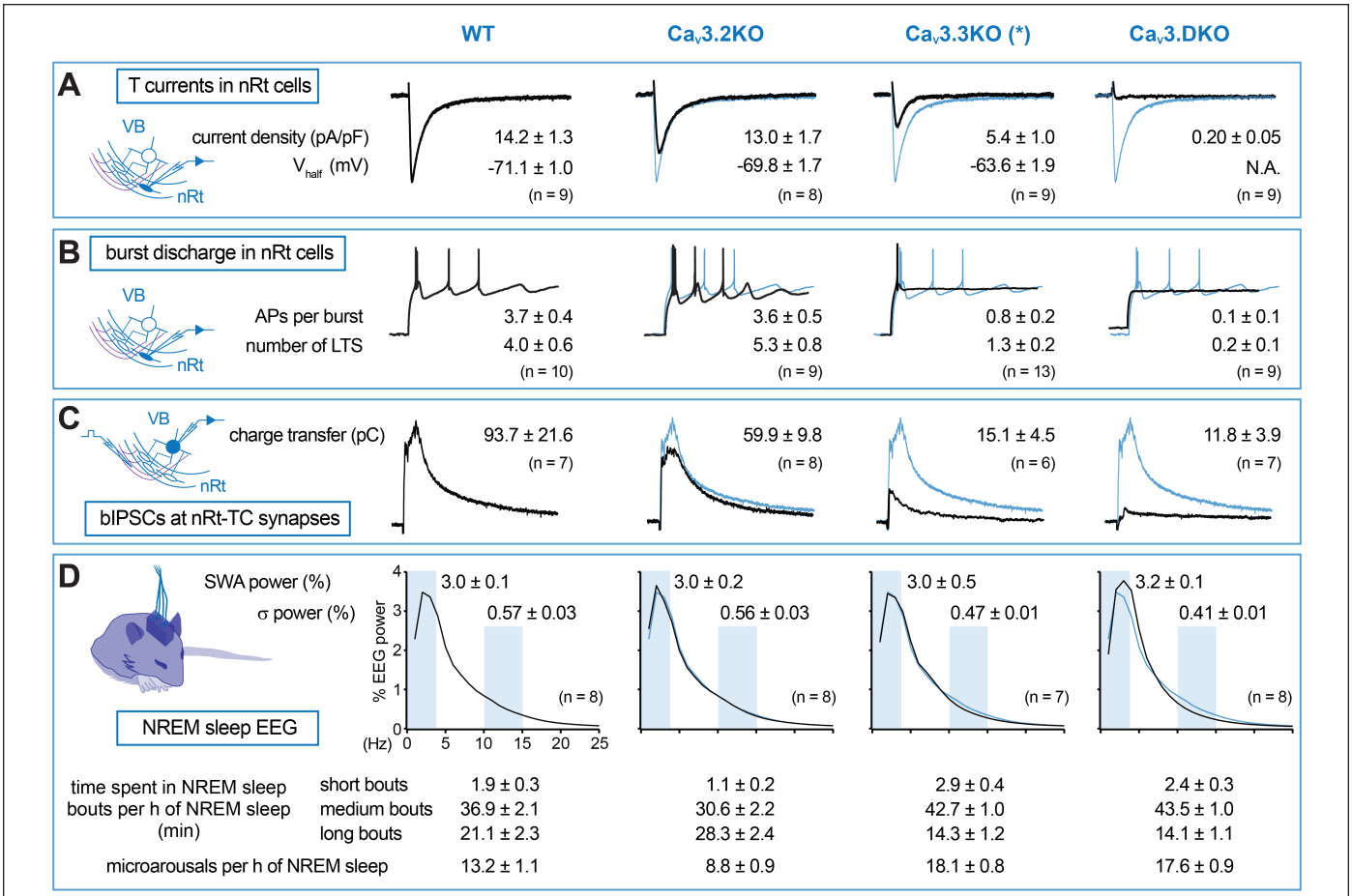

Figure 7—Summary of cellular and sleep data from mice with genetic deletions of Ca_V3 genes. **(A)** Low-threshold Ca^{2+} currents (T-currents) elicited in nRt cells by somatic depolarization are strongly reduced by *$Ca_V3.3$* single and *$Ca_V3.2xCa_V3.3$* double ablation (Ca_V3.DKO). Traces show representative T-currents in all genotypes generated by a +40 mV depolarizing step from −100 mV holding potential. Mean values for T-current density (+40 mV depolarization) and for V_{half} (estimated from the whole activation curve) are specified for each genotype. **(B)** The repetitive low-threshold bursting elicited in nRt cells at the offset of somatic current injections is preserved in $Ca_V3.2$KO mice, strongly impaired in $Ca_V3.3$KO mice, and completely abolished in Ca_V3.DKO mice. Traces are representative burst discharges in all genotypes, generated by a 400-ms-long hyperpolarization of −500 pA from −60 mV. Mean values for number of action potentials (APs) within the first burst and number of repetitive low-threshold Ca^{2+} spikes (LTS) are reported. **(C)** Ca_V3 channels differentially contribute to the inhibitory postsynaptic currents elicited in TC cells by burst discharge (bIPSCs) of nRt cells, which is evoked by electric stimulation of glutamatergic afferents. *$Ca_V3.2$* deletion partially reduces multiphasic currents, which are abolished by additional *$Ca_V3.3$* ablation. Average values of inhibitory charge transfer (generated by stimuli of 250–300 μA) are reported on top of representative bIPSCs. **(D)** Power spectra of NREM sleep are not altered in $Ca_V3.2$KO mice. *$Ca_V3.3$* deletion causes a selective reduction in the σ frequency range (10–15 Hz), which becomes more pronounced in case of *$Ca_V3.2xCa_V3.3$* ablation. Additionally, Ca_V3.DKO mice exhibit a marked increase in EEG power in the δ frequency range (2–4 Hz). Normalized NREM sleep EEG power spectrum between 0.75 and 25 Hz are shown, with shaded boxes indicating relevant intervals of frequency: SWA (0.75–4 Hz) and σ (10–15 Hz) and average values on the top. Bottom, mean values of time spent in short (< 32 s), intermediate (32–252 s), and long (> 252 s) episodes of NREM sleep and number of microarousals per hour of NREM sleep, indicating that *$Ca_V3.3$* deletion is sufficient to cause deficits in sleep consolidation. In each panel, the scheme on the left represents the recording configuration, and the blue traces on the right are wild-type data superimposed on the traces from the other genotypes for comparison. (*) $Ca_V3.3$KO data are reported from reference[17]. The NREM sleep power spectrum is presented here with normalized % values.

$Ca_V3.2$ channels, as opposed to a constitutive function of the dominating $Ca_V3.3$ channels, would be consistent with the well-documented sensitivity of the $Ca_V3.2$ channel to redox agents and to intracellular kinases[19] and might be important for use-dependent regulation of thalamocortical oscillations. An interesting open question is whether distinct Ca_V3 channel subunits are differentially recruited by cortical and thalamic glutamatergic inputs impinging onto nRt dendrites, thus modulating the feed-forward inhibition of TC cells in a subtype-specific manner.

Whereas $Ca_V3.3$-KO nRt cells showed a residual low-threshold Ca^{2+} spike carried by $Ca_V3.2$ channels,[17] Ca_V3.DKO mice displayed a complete lack of dendritic T-currents and rebound oscillatory bursting. This resulted in the abolishment of bIPSCs in TC cells, predicting disturbances in thalamic rhythms.[29] The striking effects on nRt excitability and intrathalamic synaptic transmission were indeed reflected by changes in the EEG sleep profile of Ca_V3.DKO mice. Corroborating our previous studies on the role of $Ca_V3.3$ channels in σ power, we found again a marked decrease in the σ power

surge when both Ca_V3 channel subtypes are lacking. Additionally, Ca_V3.DKO mice also showed a reduced σ band in the normalized NREM sleep power spectrum. This suggests a more pronounced impairment in sleep spindle rhythmogenesis, as compared to Ca_V3.3KO mice, which is consistent with the full disappearance of bIPSCs in the DKOs. Comparison of cellular and sleep data from this study and from our previous report on Ca_V3.3KO mice[17] reveals how the progressive impairment in nRt and intrathalamic excitability caused by *$Ca_V3.2$* and *$Ca_V3.3$* single and double ablation is accompanied by increasing deficits in NREM sleep power characteristics (Figure 7). Notably, Ca_V3.3KO mice and Ca_V3.DKO mice present a similar rearrangement of NREM sleep bouts and a higher incidence of microarousals, as compared to wild-type and Ca_V3.2KO animals, indicating that Ca_V3.3 deletion is largely sufficient to deregulate sleep consolidation. Surprisingly, Ca_V3.2KO mice appear to have more consolidated NREM sleep, with bouts of longer duration less frequently interrupted by microarousals. Notably, Ca_V3.2KO mice spent less time in NREM sleep during the dark phase, suggesting a compensatory upregulation of NREM sleep duration during the light phase. The reason for this difference during the active phase is likely to be independent of thalamocortical rhythmogenesis. Ca_V3.2 channels are highly expressed in the basal ganglia circuit, in limbic and in cortical areas.[10] Constitutive deletion of this channel has been reported to generate phenotypes not directly related to thalamocortical rhythmogenesis, such as elevated anxiety and impaired memory.[38–40] Interestingly, concomitant deletion of Ca_V3.3 channels appears to override the effect of single Ca_V3.2 channel deletion on NREM sleep bout distribution. This indicates that the lack of the major T channel subtype for nRt rhythmogenesis imposes a dominant effect of impaired thalamocortical rhythmogenesis on sleep architecture.

In Ca_V3.DKO mice, the EEG-related phenotype was not specific to the σ range, but extended to EEG power between 2–4 Hz, belonging to the δ band, which was augmented. As a result, the balance between intrathalamic networks, providing the basis for sleep spindles, and thalamocortical circuitry, implicated in SWA, was affected more severely in the Ca_V3.DKO mice. Indeed, it has been previously shown that σ and δ power are negatively correlated during NREM sleep,[41–43] which was explained by a greater extent of membrane hyperpolarization of TC cells during δ rhythm generation in deep NREM sleep that precluded spindle rhythmicity. This current work now observes such a σ-δ power opposition through genetic means and suggests that the level of nRt excitability through Ca_V3 channels and the resulting bIPSC generation is a decisive factor for the σ/δ ratio apparent in the EEG.

Contrary to what would be expected from studies on pharmacological blockade of $GABA_A$R-mediated transmission in thalamic nuclei, Ca_V3.DKO mice did not display aberrant hypersynchronous rhythms, such as the 3 Hz spike-and-wave discharge.[29,44] The emergence of these pathological oscillations was explained by a disinhibition of thalamic nuclei.[44,45] Such hyperoscillations did not take place in the Ca_V3.DKO mice because GABAergic transmission in intrathalamic circuitry was not fully abolished, and some level of inhibition through tonic nRt discharge remained. Nevertheless, the imbalance between glutamatergic and GABAergic input onto TC cells in Ca_V3.DKO mice could favor intrinsic rhythmicity of TC neurons in the δ range at the expense of 10 Hz-nRt-TC reverberations.

Despite the augmented contribution of δ waves, sleep was more fragmented in Ca_V3.DKO mice. These mice spent globally more time in NREM sleep than wild-type animals, but in episodes of shorter duration. The concomitant increase in waking bouts of short duration and the higher occurrence of microarousals support the conclusion that Ca_V3.DKO mice experienced a more fragmented sleep, which is consistent with the well-established link between spindles and sleep consolidation.[32] These data also support the view that manipulation of spindles can alter sleep architecture independently of δ waves, as previously reported in mice with a genetic overexpression of small-conductance type 2 K^+ channels, which improved sleep quality without altering SWA.[46]

Altogether, deletion of the additional source of low-threshold Ca^{2+} spike in nRt cells aggravated the sleep phenotype of Ca_V3.3KO mice, indicating a role of Ca_V3.2 channels in boosting nRt cell excitability and rhythmogenesis. Thus, the Ca_V3.DKO mice might represent a valuable model to study the involvement of nRt rhythmogenesis in pathophysiology, as already reported in the case of absence epilepsy.[27] The clinical relevance of Ca_V3.DKO mice remains a subject of further studies. Intriguingly, the deficits in sleep spindles strongly hint at the presence of a schizophrenic endophenotype.[47]

REFERENCES

1. Beenhakker MP, Huguenard JR. Neurons that fire together also conspire together: is normal sleep circuitry hijacked to generate epilepsy? Neuron 2009;62:612–32.
2. Crunelli V, Cope DW, Hughes SW. Thalamic T-type Ca^{2+} channels and NREM sleep. Cell Calcium 2006;40:175–90.
3. Cueni L, Canepari M, Adelman JP, Lüthi A. Ca^{2+} signaling by T-type Ca^{2+} channels in neurons. Pflügers Arch 2009;457:1161–72.
4. Ly R, Bouvier G, Schonewille M, et al. T-type channel blockade impairs long-term potentiation at the parallel fiber-Purkinje cell synapse and cerebellar learning. Proc Natl Acad Sci U S A 2013;110:20302–7.
5. Otsu Y, Marcaggi P, Feltz A, et al. Activity-dependent gating of calcium spikes by A-type K^+ channels controls climbing fiber signaling in Purkinje cell dendrites. Neuron 2014;84:137–51.
6. Egger V, Svoboda K, Mainen ZF. Dendrodendritic synaptic signals in olfactory bulb granule cells: local spine boost and global low-threshold spike. J Neurosci 2005;25:3521–30.
7. Becker AJ, Pitsch J, Sochivko D, et al. Transcriptional upregulation of $Ca_V3.2$ mediates epileptogenesis in the pilocarpine model of epilepsy. J Neurosci 2008;28:13341–53.
8. Shin HS, Cheong EJ, Choi S, Lee J, Na HS. T-type Ca^{2+} channels as therapeutic targets in the nervous system. Curr Opin Pharmacol 2008;8:33–41.
9. Perez-Reyes E. Molecular physiology of low-voltage-activated T-type calcium channels. Physiol Rev 2003;83:117–61.
10. Talley EM, Cribbs LL, Lee JH, Daud A, Perez-Reyes E, Bayliss DA. Differential distribution of three members of a gene family encoding low voltage-activated (T-type) calcium channels. J Neurosci 1999;19:1895–911.
11. Liu XB, Murray KD, Jones EG. Low-threshold calcium channel subunit $Ca_V3.3$ is specifically localized in GABAergic neurons of rodent thalamus and cerebral cortex. J Comp Neurol 2011;519:1181–95.
12. Fuentealba P, Steriade M. The reticular nucleus revisited: intrinsic and network properties of a thalamic pacemaker. Prog Neurobiol 2005;75:125–41.

13. Anderson MP, Mochizuki T, Xie J, et al. Thalamic $Ca_V3.1$ T-type Ca^{2+} channel plays a crucial role in stabilizing sleep. Proc Natl Acad Sci U S A 2005;102:1743–8.
14. Lee J, Kim D, Shin HS. Lack of delta waves and sleep disturbances during non-rapid eye movement sleep in mice lacking $\alpha 1_G$-subunit of T-type calcium channels. Proc Natl Acad Sci U S A 2004;101:18195–9.
15. Dossi RC, Nuñez A, Steriade M. Electrophysiology of a slow (0.5-4 Hz) intrinsic oscillation of cat thalamocortical neurones in vivo. J Physiol 1992;447:215–34.
16. Leresche N, Jassik-Gerschenfeld D, Haby M, Soltesz I, Crunelli V. Pacemaker-like and other types of spontaneous membrane potential oscillations of thalamocortical cells. Neurosci Lett 1990;113:72–7.
17. Astori S, Wimmer RD, Prosser HM, et al. The $Ca_V3.3$ calcium channel is the major sleep spindle pacemaker in thalamus. Proc Natl Acad Sci U S A 2011;108:13823–8.
18. Joksovic PM, Nelson MT, Jevtovic-Todorovic V, et al. $Ca_V3.2$ is the major molecular substrate for redox regulation of T-type Ca^{2+} channels in the rat and mouse thalamus. J Physiol 2006;574:415–30.
19. Iftinca MC, Zamponi GW. Regulation of neuronal T-type calcium channels. Trends Pharmacol Sci 2009;30:32–40.
20. Bourinet E, Alloui A, Monteil A, et al. Silencing of the $Ca_V3.2$ T-type calcium channel gene in sensory neurons demonstrates its major role in nociception. EMBO J 2005;24:315–24.
21. Liao YF, Tsai ML, Chen CC, Yen CT. Involvement of the $Ca_V3.2$ T-type calcium channel in thalamic neuron discharge patterns. Mol Pain 2011;7:43.
22. Sekiguchi F, Kawabata A. T-type calcium channels: functional regulation and implication in pain signaling. J Pharmacol Sci 2013;122:244–50.
23. Chen CC, Lamping KG, Nuno DW, et al. Abnormal coronary function in mice deficient in α_{1H} T-type Ca^{2+} channels. Science 2003;302:1416–8.
24. Cueni L, Canepari M, Luján R, et al. T-type Ca^{2+} channels, SK2 channels and SERCAs gate sleep-related oscillations in thalamic dendrites. Nat Neurosci 2008;11:683–92.
25. Astori S, Lüthi A. Synaptic Plasticity at Intrathalamic Connections via $Ca_V3.3$ T-type Ca^{2+} channels and GluN2B-containing NMDA receptors. J Neurosci 2013;33:430–4.
26. Franken P, Malafosse A, Tafti M. Genetic variation in EEG activity during sleep in inbred mice. Am J Physiol 1998;275:R1127–37.
27. Lee SE, Lee J, Latchoumane C, et al. Rebound burst firing in the reticular thalamus is not essential for pharmacological absence seizures in mice. Proc Natl Acad Sci U S A 2014;111:11828–33.
28. Joksovic PM, Bayliss DA, Todorovic SM. Different kinetic properties of two T-type Ca^{2+} currents of rat reticular thalamic neurones and their modulation by enflurane. J Physiol 2005;566:125–42.
29. Rovó Z, Mátyás F, Barthó P, et al. Phasic, nonsynaptic GABA-A receptor-mediated inhibition entrains thalamocortical oscillations. J Neurosci 2014;34:7137–47.
30. Herd MB, Brown AR, Lambert JJ, Belelli D. Extrasynaptic $GABA_A$ receptors couple presynaptic activity to postsynaptic inhibition in the somatosensory thalamus. J Neurosci 2013;33:14850–68.
31. Sun YG, Wu CS, Renger JJ, Uebele VN, Lu HC, Beierlein M. GABAergic synaptic transmission triggers action potentials in thalamic reticular nucleus neurons. J Neurosci 2012;32:7782–90.
32. Astori S, Wimmer RD, Lüthi A. Manipulating sleep spindles - expanding views on sleep, memory, and disease. Trends Neurosci 2013;36:738–48.
33. Lüthi A. Sleep spindles: where they come from, what they do. Neuroscientist 2013;20:243–56.
34. McCormick DA, Bal T. Sleep and arousal: thalamocortical mechanisms. Annu Rev Neurosci 1997;20:185–215.
35. Steriade M. Grouping of brain rhythms in corticothalamic systems. Neuroscience 2006;137:1087–106.
36. McKay BE, McRory JE, Molineux ML, et al. Ca_V3 T-type calcium channel isoforms differentially distribute to somatic and dendritic compartments in rat central neurons. Eur J Neurosci 2006;24:2581–94.
37. Warren RA, Jones EG. Maturation of neuronal form and function in a mouse thalamo-cortical circuit. J Neurosci 1997;17:277–95.
38. Chen CC, Shen JW, Chung NC, Min MY, Cheng SJ, Liu IY. Retrieval of context-associated memory is dependent on the $Ca_V3.2$ T-type calcium channel. PLoS One 2012;7:e29384.
39. Chung NC, Huang YH, Chang CH, et al. Behavior training reverses asymmetry in hippocampal transcriptome of the $Ca_V3.2$ knockout mice. PLoS One 2015;10:e0118832.
40. Gangarossa G, Laffray S, Bourinet E, Valjent E. T-type calcium channel $Ca_V3.2$ deficient mice show elevated anxiety, impaired memory and reduced sensitivity to psychostimulants. Front Behav Neurosci 2014;8:92.
41. Nuñez A, Curro Dossi R, Contreras D, Steriade M. Intracellular evidence for incompatibility between spindle and delta oscillations in thalamocortical neurons of cat. Neuroscience 1992;48:75–85.
42. Uchida S, Maloney T, March JD, Azari R, Feinberg I. Sigma (12-15 Hz) and delta (0.3-3 Hz) EEG oscillate reciprocally within NREM sleep. Brain Res Bull 1991;27:93–6.
43. Vyazovskiy VV, Achermann P, Borbély AA, Tobler I. The dynamics of spindles and EEG slow-wave activity in NREM sleep in mice. Arch Ital Biol 2004;142:511–23.
44. Castro-Alamancos MA. Neocortical synchronized oscillations induced by thalamic disinhibition in vivo. J Neurosci 1999;19:RC27.
45. Paz JT, Bryant AS, Peng K, et al. A new mode of corticothalamic transmission revealed in the $Gria4^{-/-}$ model of absence epilepsy. Nat Neurosci 2011;14:1167–73.
46. Wimmer RD, Astori S, Bond CT, et al. Sustaining sleep spindles through enhanced SK2-channel activity consolidates sleep and elevates arousal threshold. J Neurosci 2012;32:13917–28.
47. Ferrarelli F, Tononi G. The thalamic reticular nucleus and schizophrenia. Schizophr Bull 2011;37:306–15.

ACKNOWLEDGMENTS

The authors are grateful to Kevin P. Campbell for the permission of using the $Ca_V3.2$ knock-out mouse line, and to Heinz Beck for providing animal breeders. We thank Laura M.J. Fernandez for help with data analysis and Thi Dung Hau Iuliano-Dao for mouse genotyping.

SUBMISSION & CORRESPONDENCE INFORMATION

Submitted for publication June, 2015
Submitted in final revised form October, 2015
Accepted for publication October, 2015
Address correspondence to: Simone Astori, PhD or Anita Lüthi, PhD, Department of Fundamental Neurosciences, University of Lausanne, Rue du Bugnon 9, CH-1005 Lausanne; Tel: +41 21 692 5294; Fax: +41 21 692 5105; Email: simone.astori@unil.ch or anita.luthi@unil.ch

DISCLOSURE STATEMENT

This was not an industry supported study. This work was supported by the Swiss National Science Foundation (Ambizione grant PZ00P3_136761 to S.A. and grant 31003A-146244 to A.L.) and Etat de Vaud. The authors have indicated no financial conflicts of interest.